Electron scattering at surfaces and grain boundaries in Cu thin films and wires

J. S. Chawla,[1] F. Gstrein,[2] K. P. O'Brien,[2] J. S. Clarke,[2] and D. Gall[1,*]

[1]*Department of Materials Science and Engineering, Rensselaer Polytechnic Institute, Troy, New York 12180, USA*

[2]*Intel Corporation, 5200 N.E. Elam Young Parkway, Hillsboro, Oregon 97124-6497, USA*

(Received 24 June 2011; revised manuscript received 16 November 2011; published 5 December 2011)

The electron scattering at surfaces, interfaces, and grain boundaries is investigated using polycrystalline and single-crystal Cu thin films and nanowires. The experimental data is described by a Fuchs–Sondheimer (FS) and Mayadas–Shatzkes (MS) model that is extended to account for the large variation in the specific resistivity of different grain boundaries as well as distinct top and bottom surfaces with different scattering specularity p. Textured polycrystalline Cu(111) thin films with thickness $d = 25$–50 nm are deposited on a stack of 7.5-nm Ta on SiO_2/Si(001). Subsequent annealing results in small-grain (SG) thin films with an average grain size $\bar{D}$ that increases from 90 to 120 nm with increasing d. Corresponding large-grain (LG) thin films with $\bar{D} = 160$–220 nm are obtained by depositing 100–200-nm-thick films, followed by an *in-situ* anneal and a subsequent etch to match the thickness of the SG samples. Nanowires are fabricated from the SG and LG thin films using a subtractive patterning process, yielding wire widths of 75–350 nm. Single-crystal and LG layers exhibit a 18–22% and 10–15% lower resistivity than SG layers, respectively. The resistivity decrease from SG to LG Cu nanowires is 7–9%. The thickness and grain size dependence of the resistivity of polycrystalline and single-crystal Cu layers is well described by an exact version of the existing FS + MS model but is distinct from the commonly used approximation, which introduces an error that increases with decreasing layer thickness from 6.5% for $d = 50$ nm to 17% for $d = 20$ nm. The case of nanowires requires the FS + MS model to be extended to account for variation in the grain boundary reflection coefficient R, which effectively increases the overall resistivity by, for example, 16% for 50×45 nm^2 wires. The overall data from single and polycrystalline Cu layers and wires yields $R = 0.25 \pm 0.05$, and $p = 0$ at Cu-air and Cu-Ta interfaces.

DOI: 10.1103/PhysRevB.84.235423 PACS number(s): 72.15.−v, 72.10.Fk

I. INTRODUCTION

The classical size effect refers to the increase in the resistivity of metal films and wires as their critical dimensions (thickness of film, width and height of wires) approach or become less than the electron mean free path λ, which is 39 nm for bulk copper at room temperature.[1] This size effect is currently of great concern to the semiconductor industry as Cu interconnect wires are now in this size effect regime.[2] For example, the resistivity of a 40-nm-wide Cu wire is reported to be 2.5 times higher than for bulk Cu.[3,4] The most studied electron scattering mechanisms that lead to the size effect in Cu are (1) scattering at external surfaces or interfaces, which causes an increase in the resistivity of interconnect lines as the thickness d_{Cu} and/or the line width w decrease; (2) scattering at grain boundaries, which typically increase in density with decreasing d_{Cu}; and (3) surface roughness, which reduces the effective cross-sectional area of interconnect lines.[5] The convolution of these effects makes the development of a detailed quantitative understanding of electron scattering mechanisms in Cu interconnects challenging.

A theoretical description of the resistivity increase of thin metal layers with decreasing thickness was developed by Fuchs and Sondheimer (FS).[6,7] Their well-known size-effect theory describes classic electron surface scattering events as either diffuse or specular and are quantified by the specularity parameter p ($0 < p < 1$), which the FS model assumes to be equal for both top and bottom surfaces of a metallic layer. Specular scattering ($p = 1$) refers to an elastic scattering event where the electron momentum perpendicular to the surface is reversed, while the parallel component is conserved, causing no effect on the resistivity. In contrast, diffuse scattering ($p = 0$) results in a complete randomization of the electron momentum and a corresponding increase in the resistivity. Surface scattering processes and, in turn, values for p are affected by charge density variations associated with atomic level surface roughness[8–11] and the interface with other atoms and molecules,[12–16] which are typically different for the top and bottom surfaces. We reported earlier,[10] using a derivation comparable to FS, the expression for the resistivity ρ_s of a single-crystal metal layer of thickness d with top and bottom surfaces with different specularity parameters p_1 and p_2:

$$\rho_s = \rho_o\left[1 - \frac{3}{4\kappa}\int_1^{\infty}\left(\frac{1}{t^3} - \frac{1}{t^5}\right)\frac{2(1 - p_1p_2e^{-\kappa t})(1 - e^{-\kappa t}) - (p_1 + p_2)(1 - e^{-\kappa t})^2}{1 - p_1p_2e^{-2\kappa t}}dt\right]^{-1} \quad (1)$$

where $\kappa = d/\lambda$ and $\rho_\circ$ is the bulk resistivity.

 ©2011 American Physical Society

For the case of polycrystalline layers, the contribution of grain boundary scattering on the size effect needs to be considered as well. For this purpose, Mayadas *et al.* (MS) derived the following expression for the intrinsic resistivity of a metal thin film with columnar grains with an average lateral grain size D:[17]

$$\rho_g = \rho_o \left[1 - \frac{3}{2}\alpha + 3\alpha^2 - 3\alpha^3 \ln\left(1 + \frac{1}{\alpha}\right)\right]^{-1} \quad (2)$$

where $\alpha = \frac{\lambda}{D}(\frac{R}{1-R})$ and R $(0 < R < 1)$ is the reflection coefficient of electrons scattering at the grain boundaries perpendicular to the current flow. Other theoretical descriptions of the size effect typically build on the surface and grain boundary models by FS and MS, respectively. For example, Soffer[18] uses the roughness of the scattering surface to calculate an angle-dependent specular reflection probability, and Rossnagel and Kuan[8] use Monte Carlo simulations of electron trajectories to derive parameters that describe the geometrical impact of surface roughness.

For the case of nanowires, a quantitative understanding of scattering effects is further complicated by scattering on four (instead of two) external surfaces, the presence of two independent dimensional parameters (width and height), anisotropic grain sizes in the two directions perpendicular to the current flow, and grain formation that depends on the wire fabrication process. Similar to thin films, the resistivity increase in metal nanowires is attributed to surface and grain boundary scattering, as well as defect and impurity scattering.[4,19,20] However, the relative contributions are less known and models for nanowires are less developed than for thin films.

Various experimental studies on polycrystalline Cu thin films and wires use FS- and MS-based models to analyze their experimental data. The constants p and R are free and independent fitting parameters[8,21–24] and determine the relative contribution of surface and grain boundary scattering, respectively. Most studies find $p \approx 0$ at all Cu interfaces,[8,21,25] corresponding to completely diffuse surface scattering, and $0.2 < R < 0.5$.[3,26,27] However, the interdependence and the uncertainty in the quantification of grain size, thickness, and roughness of the Cu layers complicates the determination of p and R from any set of polycrystalline samples. For example, the resistivity of 230-nm-high and 40–800-nm-wide Cu wires with grain sizes assumed to be equal to the smallest dimension of the wires can be fit equally well with parameter pairs of ($p = 1$, $R = 0.53$), ($p = 0.6$, $R = 0.5$), and ($p = 0$, $R = 0.43$).[3,26] Recently, Sun *et al.* determined that grain boundary scattering dominates over surface scattering for polycrystalline 35–425-nm-thick Cu layers with equivalent top and bottom surfaces and grains that are 2 times larger than the film thickness, using measured thickness, grain size, and resistivity data at 300 and 4.2 K.[23,28] In contrast, Munoz *et al.* and Henriquez *et al.* conclude that electron surface scattering is the dominant electron scattering mechanism for 50-nm-thick Au layers with grains that are approximately 2 times larger than the film thickness, but grain boundary scattering becomes dominant if the grain size is reduced to approximately 0.2 times the film thickness, as determined from measured thickness, grain size distribution, temperature-dependent electrical resistivity, and Hall mobility at 4 K.[29–31] A further complication in the mechanistic understanding of grain boundary scattering is that the specific resistivity of Cu grain boundaries varies by 1–2 orders of magnitude, depending on its structural symmetry and coherence.[20,32] This effectively increases the apparent average grain boundary reflection coefficient in narrow wires where the current is forced to cross both high- and low-resistivity boundaries, while (in contrast) the current in a film preferentially flows only across low-resistivity boundaries.

In order to quantify grain boundary and surface scattering in Cu thin films and nanowires, the following experimental conditions must be met: (i) The specularity parameter p for all interfaces are determined using single crystal Cu films. Such data is most reliable for single-crystal layers since grain boundary scattering is absent. (ii) The grain size of polycrystalline films is varied independently of film thickness in order to deconvolute grain size and thickness effects. (iii) The critical dimensions of thin films and nanowires as well as grain size and surface roughness are characterized by independent techniques. This paper is motivated by these requirements and is based on a combination of Fuchs–Sondheimer (FS) and Mayadas–Shatzkes (MS) models. First, this paper determines the surface scattering parameters for the Cu-vacuum, Cu-air, and Cu-Ta interfaces from single-crystal Cu(001)/MgO(001) layers. This data is then used to minimize fitting uncertainty for polycrystalline Cu conductors. Secondly, the grain boundary scattering parameter for Cu is determined using polycrystalline thin films with variable thickness $d_{Cu} = 25$–50 nm. The grain size for these layers is statistically analyzed and varied by a factor of 1.8 while keeping the thickness constant. Lastly, the grain boundary scattering parameter for 70–350-nm-wide and 45-nm-thick nanowires is determined. All experimental data is interpreted using a formalism that combines the FS and MS models and includes new additional terms to account for the distinct top and bottom layer surfaces and the large variation in the specific resistivity of different grain boundaries along the wire. This model deviates from Matthiessen's rule, as discussed in the theoretical section of this paper, and quantified in Sec. IV C.

II. EXPERIMENTAL PROCEDURE

Cu layers were deposited at 298 K in a 300-mm wafer physical vapor deposition tool with a base pressure of 10^{-8} Torr on Ta/SiO_2/Si(001) substrates, where the SiO_2 is a 100-nm-thick thermally grown oxide and the Ta is a 7.5-nm-thick Ta underlayer that is *in-situ* sputter deposited at 298 K immediately prior to the Cu deposition. After deposition, all Cu layers were annealed *in-situ* at 623 K for 10 minutes without breaking the vacuum, resulting in growth of the Cu grains to sizes that are approximately proportional to the deposited film thickness d_o. Small-grain (SG) samples were prepared by depositing relatively thin layers of Cu with thickness ranging from 25 to 50 nm. Large-grain (LG) samples were obtained by deposition of thick Cu layers ($d_o = 100$–200 nm) followed by Ar ion sputter etching to yield layers with thickness matched to those of the SG samples. The Ar^+ plasma had an etch rate of 2.5 Å/s, and wafers were electrostatically chucked and actively cooled with backside gas during the etch to keep wafers at ~298 K. In addition, single-crystal Cu(001) layers with

d_{Cu} = 21, 27, and 40 nm were deposited on MgO(001) substrates by dc magnetron sputtering, using a deposition system with a base pressure of 10^{-9} Torr following the procedure in Refs. 10 and 33. The layer thickness was measured during deposition by a quartz crystal microbalance and after fabrication by optical interferometry (OFT) and x-ray reflectivity (XRR) analyses. Cu wires of various line widths ranging from 70 to 350 nm, as well as contact pads in a linear 4-point probe geometry, were fabricated by e-beam lithography using a negative resist followed by Ar^+ ion sputter etching. The crystallinity, texture, and grain orientations of blanket films were quantified by x-ray diffraction (XRD) using a Panalytical X'pert PRO MPD system with a Cu Kα source, a two-crystal Ge(220) two-bounce monochromator yielding monochromatic Cu Kα_1 radiation with 0.0068° divergence for θ-2θ and ω-rocking scans, and a point focus x-ray lens (polycapillary optics) that provides a quasiparallel Cu Kα beam with a divergence <0.3° for pole-figure texture measurements.

Electron backscatter diffraction (EBSD) was employed to map the grain size and orientation distribution. They are visualized with color-coded grain orientation maps. Cu surface areas of 100–400 μm^2 were analyzed, corresponding to 5000–10 000 grains per analyzed sample. This grain number is well above the minimum of 1000 or 500 grains required to obtain an accurate grain size distribution, according to Refs. 28 and 34, respectively. The maps were obtained using a step size ~1/10th of the nominal grain size to optimize EBSD mapping speed and minimize error in mean grain diameter measurements. Humpherys[35] reported that EBSD step size, which is 1/8th of the nominal grain size, results in less than 5% error in the mean grain size determination. The area of each grain in the EBSD map is determined by multiplying the area per measurement (that is, the square of the step size) with the number of adjacent data points for which the orientation varies overall by less than 10°. The grain size D is then defined as the diameter of a circle with the same area as the grain area. Throughout this paper, the grain size D refers to the size in the plane parallel to the substrate surface. Thus, it does not consider the grain extension perpendicular to the substrate, which is equal to the layer thickness. Electron backscatter diffraction measurements were performed one week after Cu deposition and annealing to give enough time for possible room temperature grain growth[36] to occur prior to characterization.

The electrical resistivity of the Cu thin films was measured using a linear 4-point probe technique in ambient at 298 K, and the wires were measured in vacuum (~10^{-5} Torr) at 250–340 K. The temperature dependence of the resistivity for the wires was used to determine the effective cross-sectional area and hence the line width using the corresponding layer thickness, assuming a rectangular cross section. The line width data was also verified, with 10% accuracy, by cross-sectional scanning electron microscopy (SEM).

III. THEORETICAL FRAMEWORK

The resistivity measurements for Cu films and wires are discussed within the theoretical framework by Fuchs and Sondheimer (FS) for electron scattering at surfaces and by Mayadas and Shatzkes (MS) for electron scattering at grain boundaries, see Eqs. (1) and (2), respectively. We use a similar approach as MS[22] to derive the total resistivity ρ_f of a metal layer of thickness d in which there is simultaneous electron scattering from an isotropic background (due to combined effects of phonons and bulk defects), grain boundaries, and distinct top and bottom surfaces with specularity parameters p_1 and p_2:

$$\rho_f = \left\{ \frac{1}{\rho_g} - \frac{3}{\pi\kappa\rho_o} \int_0^{\pi/2} d\phi \int_1^{\infty} dt \frac{\cos^2\phi}{H^2(t,\phi)} \left(\frac{1}{t^3} - \frac{1}{t^5}\right) \frac{2[1-p_1p_2e^{-\kappa t H(t,\phi)}][1-e^{-\kappa t H(t,\phi)}] - (p_1+p_2)[1-e^{-\kappa t H(t,\phi)}]^2}{1-p_1p_2e^{-2\kappa t H(t,\phi)}} \right\}^{-1}. \tag{3}$$

Here, $H(t,\phi) = 1 + \frac{\alpha}{\cos\phi}(1-\frac{1}{t^2})^{1/2}$, α, and κ were introduced along with Eqs. (1) and (2), and ρ_g is the grain boundary resistivity in case of completely specular surface scattering as defined in Eq. (2). Equation (3) is derived using a distinct relaxation time to describe the electron scattering from an isotropic background and from grain boundaries, whereas the electron scattering from external surfaces is represented not by a relaxation time but by boundary conditions on the electron distribution $\Phi^{\pm}(v_z,z)$ along the transverse direction z for $v_z > 0(+)$ and $v_z < 0(-)$: $\Phi^+(v_z,0) = p_1\Phi^-(-v_z,0)$, and $\Phi^-(v_z,d) = p_2\Phi^+(-v_z,d)$. This boundary condition is similar to that used by the originally reported MS and FS derivation,[6,22] but differs in that it uses two separate interface specularity parameters p_1 and p_2 for top and bottom surfaces. A corollary to Eq. (3) is a deviation from Matthiessen's rule,[22] since Matthiessen's rule assumes that all relevant scattering mechanisms can be represented by individual and independent relaxation times and that electron scattering rates and resistivities are additive. This is definitely not the case for Eq. (3). It is difficult, however, to observe the deviation from Matthiessen's rule experimentally because the magnitude of the deviation, as quantified in Sec. IV C, is comparable to the experimental uncertainty. In fact, recent electron transport results from our laboratory suggest that deviations from Matthiessen's rule for phonon and surface scattering are too small to be experimentally observed, for the case of 4–1400-nm-thick single-crystal Cu layers at 298 and 77 K.[37] A convenient approximation to Eq. (3) can be derived for the limiting case of $\kappa \gg 1$ and $\alpha \ll 1$:

$$\rho_{b+g+s} = \rho_o + \frac{3\rho_o}{8\kappa}\left(1 - \frac{p_1+p_2}{2}\right) + \frac{3\rho_o\alpha}{2}. \tag{4}$$

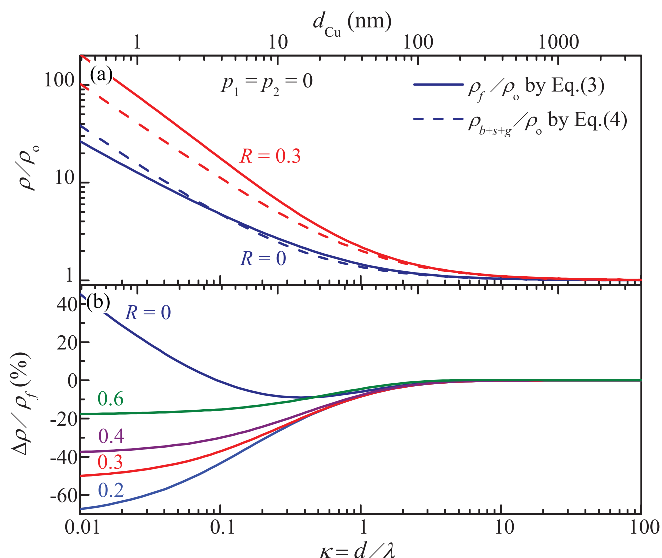

FIG. 1. (Color online) (a) Normalized layer resistivity ρ/ρ_o calculated using Eqs. (3) and (4) and a grain boundary reflection coefficient $R = 0$ and 0.3, and (b) the relative error $\Delta\rho/\rho_f = (\rho_{b+s+g} - \rho_f)/\rho_f$ where ρ_f and ρ_{b+s+g} are calculated using Eqs. (3) and (4), respectively, for different values of $R = 0$–0.6. The κ in the x axis refers to the layer thickness d normalized by the bulk electron mean free path λ, while the upper x axis indicates the thickness d_{Cu} for a room temperature Cu layer. The calculations assume the grain size D to be equal to the layer thickness and the electron surface scattering to be completely diffuse.

In this limiting case, the total resistivity corresponds to the sum of resistivities due to three scattering mechanisms, suggesting the applicability of Matthiessen's rule. In order to illustrate the parameter space over which the approximation in Eq. (4) is applicable, Fig. 1(a) shows a plot of the normalized resistivity ρ/ρ_o vs $\kappa = d/\lambda$ as calculated using the exact Eq. (3) and the approximate Eq. (4), using completely diffuse surface scattering at both surfaces, that is $p_1 = p_2 = 0$, and setting $R = 0$ and 0.3, representing typical single-crystal and polycrystalline layers, respectively. For the latter, the grain size D is set equal to the thickness d, which is a reasonable approximation for sputtered and evaporated metal layers within the thickness range 1 nm $\leqslant d \leqslant$ 1000 nm.[38] We note that Eq. (3) reduces to Eq. (1) for the case of $R = 0$. The curves overlap reasonably well for $\kappa > 1$, which corresponds to a room temperature Cu layer thickness $d_{Cu} >$ 39 nm, as indicated in the top x axis. That is, Eq. (4) is accurate for $\kappa > 1$ to within 6 and 8% for $R = 0$ and 0.3, respectively, but the accuracy decreases sharply for $\kappa < 1$. This is illustrated in Fig. 1(b), which is a plot of the relative error due to the approximation in Eq. (4) vs κ for various values of R. Equation (4) underestimates the resistivity of polycrystalline layers for all $R > 0.01$ and all $\kappa = 0.01$–100. The error increases with decreasing κ. For example, $R = 0.2$ yields a −8% error for $\kappa = 1$ but a −70% error for $\kappa = 0.01$. The relative error also decreases with increasing R (>0.01) for all κ; for example, at $\kappa = 0.1$, the relative error decreases from 45 to 0.5% as R increases from 0.2 to 0.8. However, for single-crystal layers ($R = 0$), Eq. (4) underestimates the resistivity for $\kappa > 0.1$ with a maximum error of 9% at $\kappa = 0.3$, and overestimates for $\kappa < 0.1$ with the error sharply increasing from 8 to 45% as κ decreases from 0.05 to 0.01.[39] For the analysis of the experimental data in the Results section, with $20 < d_{Cu} < 50$ nm corresponding to $0.5 < \kappa < 1.2$ at 298 K, we use exclusively the exact Eq. (3) for both single and polycrystalline Cu layers. However, the results on wires are analyzed with an extended version of the approximate expression of Eq. (4), as described in the following.

The size effect for wires has been described by Dingle,[19] who derived an approximate equation for the resistivity of rectangular single crystal wires $\rho_{wire,b+s}$ which is valid when the electron scattering occurs at all four edges with equal specularity p, and both the wire width w and height d are larger than λ:[19]

$$\frac{\rho_{wire,b+s}}{\rho_o} = 1 + \frac{3\lambda}{8}\left(\frac{1}{d} + \frac{1}{w}\right)(1-p). \quad (5)$$

In order to account for grain boundaries in polycrystalline wires, we follow the additive approach, as suggested by the approximate expression in Eq. (4), and derive

$$\rho_{wire} = \rho_o + \frac{3\lambda\rho_o}{8}\left(\frac{1}{d} + \frac{1}{w}\right)(1-p) + \frac{3\alpha\rho_o}{2}\left(1 + \frac{D}{w}\right). \quad (6)$$

This equation includes an additional semi-empirical grain boundary scattering term which accounts for the increased probability that with decreasing w a high-resistive grain boundary extends across the entire wire.[20] That is, for the case of wide wires or thin films, where $w \gg D$, the current flows around grain boundaries which exhibit a particularly large R; thus, the extra term D/w becomes negligible. However, for narrow wires, i.e. $w < D$, the boundary extends across the entire wire, and the current is forced to cross the boundary independent of its specific resistivity. This effectively increases the contribution of grain boundary scattering to the overall resistivity. In addition, the local reflection coefficient across a boundary is expected to exhibit spatial variations; thus, even a single grain boundary exhibits a higher effective R for a narrower wire because current cannot preferentially cross the boundary at positions which locally exhibit the lowest reflection coefficient. Here, we note that the grain size distribution as well as the variation in the specific boundary resistivity should, in principle, affect the proposed term D/w and could be accounted for by an additional unknown prefactor. However, for simplicity, this is omitted in this paper.

IV. RESULTS AND DISCUSSION

A. Grain size analysis

Figure 2(a) shows a representative electron backscatter diffraction (EBSD) inverse pole figure grain orientation map obtained from a LG 40-nm-thick $Cu/Ta/SiO_2/Si$ layer. It is a small portion of the total 20 × 20 μm^2 area that has been analyzed using a step size of 30 nm. The brightness/coloring corresponds to the crystal orientations as indicated in the projection shown as inset. The black lines indicate the positions of grain boundaries, which are defined as boundaries where the crystalline orientation changes by >10°. The distance

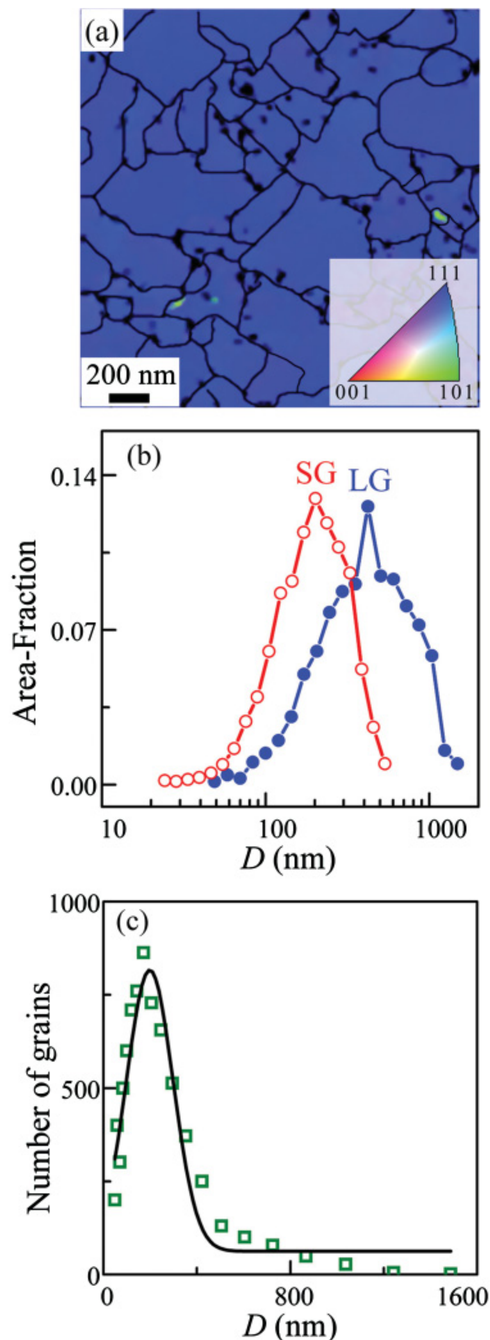

FIG. 2. (Color online) (a) Electron backscatter diffraction (EBSD) inverse pole figure grain orientation map for a 40-nm-thick LG Cu/Ta/SiO_2/Si layer. The dark contrast indicates boundaries where the crystalline orientation changes by $>10^\circ$. The inset indicates the color code for the grain orientations. (b) Area fraction grain size distribution histogram for 40-nm-thick LG and SG layers, as determined from statistical analysis of EBSD grain orientation maps. (c) Grain size histogram from the same LG layer as in (b), but plotted as number frequency vs linear size, including a Gaussian curve used for data analysis.

between such black lines corresponds to the grain sizes and ranges from 50–1500 nm, consistent with the detailed analysis described below. Based on the image in Fig. 2(a), the majority of the grains are oriented with their ⟨111⟩ axis close to the growth direction, i.e. perpendicular to the substrate surface, corresponding to a preferred ⟨111⟩ orientation. This is confirmed with a statistical analysis of a full 400-μm^2 area, indicating that 99.8% of the surface exhibits Cu grains with ⟨111⟩ orientation, and ∼0.1% with ⟨110⟩ orientation.

The grain boundary information in the EBSD orientation maps is used for statistical analyses of the grain size distributions. Figure 2(b) shows a comparison of the EBSD determined grain-size histogram plotted as area-fraction distribution in semilog scale for SG and LG 40-nm-thick Cu layers, based on the measured grain size of 7157 and 8153 grains in the two samples, respectively. Both Cu layers show a broad grain size distribution, with grain sizes ranging from 0.02 to 0.6 μm and from 0.05 to 1.5 μm for the SG and LG samples, respectively. The minimum detectable grain size depends on the measurement step size, which was 15 and 30 nm for SG and LG layers, respectively. The SG and LG layers show similar grain size distributions; however, the plot for the LG layer is shifted to the right toward larger grain sizes. The grain sizes at the histogram maxima for the SG and LG layers equal 200 and 420 nm, while the average grain sizes are $\bar{D} = 110$ and 200 nm, respectively. The average values $\bar{D}$ are obtained from the data in Fig. 2(b) using $\bar{D} = \frac{1}{N}\sum_{i=1}^{N} D_i$ where N is the total number of measured grains and D_i is the size of the ith grain. The values for $\bar{D}$ are in excellent agreement with the mean grain size of 200 ± 6 and 110 ± 4 nm, respectively, obtained by fitting the data with a Gaussian distribution. This is illustrated in Fig. 2(c), which shows a representative linear-scale histogram of the grain size number frequency for the 40-nm-thick LG Cu layer sample also presented in Figs. 2(a) and 2(b). The solid line is the Gaussian distribution curve with a fit quality of $R^2 = 0.95$. It provides values for the grain size mean and Gaussian curve width of 200 ± 6 and 190 ± 10 nm, respectively, in excellent agreement with $\bar{D} = 200$ nm from above. Similarly, the Gaussian fit for the corresponding SG Cu layer (not shown) has a similar quality of $R^2 = 0.92$ and provides mean and width values of 110 ± 4 and 120 ± 10 nm, respectively, again in excellent agreement with $\bar{D} = 110$ nm from above.

The LG layer exhibits a 1.8 times larger $\bar{D}$ than in the SG layer. This is attributed to the four times larger as-deposited layer thickness $d_o = 160$ nm, which is reduced by ion sputtering to the same thickness $d_{Cu} = 40$ nm as the SG layer. An increase in grain size with layer thickness is common for vacuum-deposited thin films and is typically described by a power law relationship.[40] Correspondingly, we describe the average grain size after annealing with a power law $\bar{D} = A d_o^{\xi}$, where d_o refers to the as-deposited thickness, with $d_{Cu} = d_o$ for SG and $d_{Cu} = d_o/4$ for LG layers. The measured grain size distribution vs d_o provides values for the prefactor $A = 22.4$ and the growth exponent $\xi = 0.43$. The latter value is close to the theoretically predicted growth exponent of 0.4 for polycrystalline growth of materials with a cubic crystal structure.[40,41] The SG and LG Cu samples with $d = 25$–50 nm, discussed in this paper, have an average grain size $\bar{D} =$ 90–120 nm and 160–220 nm, respectively, as extrapolated using the power law.

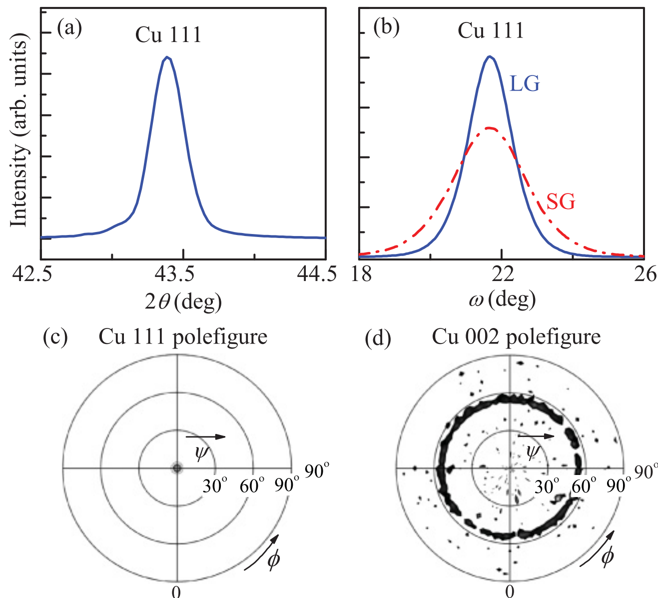

FIG. 3. (Color online) X-ray diffraction (a) θ-2θ scan about the Cu 111 peak for a 40-nm-thick LG Cu layer, (b) ω-rocking curves from the Cu 111 reflection for 40-nm-thick LG and SG layers, and (c) Cu 111 and (d) Cu 002 pole figures measured at constant $2\theta = 43.38^\circ$ and 50.42°, respectively, from a 40-nm-thick LG layer.

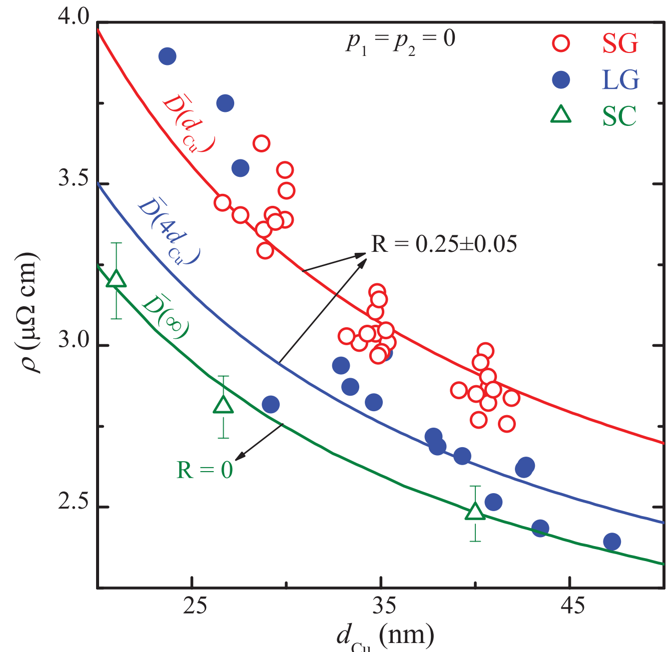

FIG. 4. (Color online) Measured resistivity ρ of Cu layers at 298 K vs thickness d_{Cu}, from polycrystalline SG and LG and single-crystal (SC) Cu layers. The solid lines are the result of a simultaneous fit with Eq. (3), using an average grain width $\overline{D}(d_o) = Ad_o^{\xi}$ with $d_o = d_{\mathrm{Cu}}$ for SG and $d_o = 4 \times d_{\mathrm{Cu}}$ for LG layers.

B. Structural characterization

Figure 3 shows representative x-ray diffraction (XRD) results of 40-nm-thick LG and SG Cu layers. For both samples, the only observable peaks in θ-2θ scans for 2θ ranging from 30° to 90° are the Cu 111 and the Si 004 reflections, indicating strong 111 preferred orientation, confirming the EBSD results. A typical Cu 111 peak is shown in Fig. 3(a), in that case from a LG 40-nm-thick Cu layer. The peak maximum is at $2\theta = 43.385^\circ$, corresponding to a measured lattice constant of $a_{\mathrm{Cu}} = 0.3609$ nm, which is 0.14% below the reported lattice constant for bulk Cu, 0.3614 nm,[42] indicating a slight biaxial tensile stress causing an in-plane strain of $\varepsilon_2 = 0.0012$ determined using a Poisson ratio $\upsilon_{\mathrm{Cu}} = 0.36$.[43] The full width at half maximum (FWHM) of the Cu 111 peak in Fig. 3(a) is 0.28°. This corresponds to an x-ray coherence length of 32 nm, which is close to the layer thickness of 40 nm, indicating little residual strain variations and/or crystalline defects within Cu grains.

Figure 3(b) shows ω-rocking curves of the Cu 111 peak at a constant $2\theta = 43.385^\circ$ for 40-nm-thick polycrystalline SG and LG Cu layers. The FWHM of the LG layer peak, 1.37°, is 1.8 times narrower than the corresponding value for the SG layer, 2.43°. This suggests that the LG samples have an approximately 1.8 times larger grain size, consistent with the EBSD measurements. The fact that the LG and SG samples have comparable peak width for θ-2θ scans (not shown) but show a systematic difference for the ω-rocking curve widths confirms that the Cu grains are columnar; that is, they all extend from the bottom to the top of the film, but they exhibit different lateral grain sizes.

Pole figure measurements confirm the clear 111-texture for all polycrystalline Cu layers. Representative Cu 111 and 002 XRD pole figures from a 40-nm-thick LG Cu film are shown in Figs. 3(c) and 3(d). They were measured at constant 2θ values corresponding to Cu 111 and Cu 002 reflections at 43.38° and 50.42°, respectively. The Cu 111 pole figure exhibits a single peak at the origin with an average FWHM along ψ of 2°. The Cu 002 pole figure shows a circular symmetric ring with a 3° width at a tilt angle $\psi = 54^\circ$. Both pole figures indicate a 111-texture.

C. Electron transport in Cu layers

Figure 4 shows plots of the room temperature resistivity ρ of Cu layers vs thickness d_{Cu}, from polycrystalline SG and LG Cu/Ta and single-crystal Cu/MgO layers. The resistivity increases with decreasing d_{Cu} for all sample sets, due to increased scattering at (1) the top Cu-air interface; (2) the bottom surface, which is a Cu-MgO or Cu-Ta interface; and (3) grain boundaries, which increase in density with decreasing d_{Cu}. The data also shows a decrease in ρ from SG to LG to single crystal Cu layers, from 2.89 to 2.65 to 2.50 $\mu\Omega$-cm at $d_{\mathrm{Cu}} = 40$ nm and from 3.45 to 3.55 to 2.81 $\mu\Omega$-cm at $d_{\mathrm{Cu}} =$ 26 nm. This is attributed to the increase in grain size from SG to LG samples, as confirmed by EBSD and XRD measurements, and hence less electron scattering at grain boundaries in LG than SG Cu layers. Similarly, the single-crystal layers have no grain boundaries and show a lower resistivity than the polycrystalline layers. The resistivity for single-crystal Cu/MgO layers, which is 18–22% lower than SG Cu/Ta layers, represents the least attainable resistivity for 25–50-nm-thick Cu layers by completely eliminating the electron scattering at grain boundaries.

The solid lines in Fig. 4 indicate the expected resistivity obtained by numerically solving Eq. (3). For this purpose,

the average grain size $\bar{D}$ for each layer is obtained from the power law which relates the measured grain size with the as-deposited layer thickness, as discussed above. In addition, the value of p_1 and p_2 for the top Cu-air boundary and the bottom Cu-Ta or Cu-MgO interfaces, respectively, is set to zero. The Cu-air and Cu-MgO interfaces are expected to yield completely diffuse electron scattering since, based on our previous results, air-exposed single-crystal Cu(001)/MgO(001) layers follow the FS prediction using Eq. (1) for completely diffuse scattering on both surfaces ($p_1 + p_2 = 0$).[9,10] This is consistent with reported *ab initio* transport calculations and experiments on single crystal Cu layers,[12] which show specular scattering at smooth *in-situ* Cu-vacuum boundaries but a resistivity increase with oxygen exposure. At an oxygen exposure equivalent to air exposure, the Cu-air boundary shows completely diffuse scattering, which is attributed to Cu oxide formation that causes atomic-level roughness of the conducting metal surface. Metallic Ta atoms at a Cu surface perturb the flat periodic potential of atomically smooth Cu, effectively introducing additional scattering centers to electron waves traveling towards this boundary and causing destructive interference of the scattered electron wave which, in turn, results in completely diffuse surface scattering,[10,44] based on our previous results from *in-situ* deposition of 0.3–7-nm Ta cap layers on the single-crystal Cu(001) surface.[10]

The expected curve for the resistivity of single-crystal (SC) layers in Fig. 4 describes the experimental data well, with deviations of only 2.4–0.8% for $d_{Cu} = 21$–40 nm. The curves for the SG and LG Cu layers on Ta are determined using simultaneous fitting, where the only fitting parameter is the grain boundary reflection coefficient R, which is found to be 0.25 ± 0.05. The curves agree reasonably well with the measured data, indicating that Eq. (3) correctly accounts for both surface and grain boundary scattering. In particular, all measured data points for SG Cu layers follow within 6% the corresponding calculated curve, while the deviation of measured and modeled resistivity for LG Cu layers increases from 4 to 19% as the thickness decreases from 50 to 20 nm. This is attributed to the ion sputter etch process on the top surface of the LG layers, which causes an increased Cu-air surface roughness, as observed by x-ray reflectivity (XRR) measurements (not shown), indicating a root mean square (rms) roughness for 40-nm-thick LG and SG Cu layers of 2.9 and 1.0 nm, respectively. An rms roughness of 2.9 nm corresponds to an 8.2-nm peak-to-valley height, which is a considerable fraction of a 40-nm-thick Cu layer, and causes, based on a formalism developed by Rossnagel and Kuan, an additional resistivity increase of 0.12 to 0.50 $\mu\Omega$-cm in 60- to 20-nm-thick Cu layers, respectively,[8,45] which corresponds to a 5–20% increase and explains the deviation of the LG data from the plotted curve in Fig. 4. The top surface rms roughness of 20- to 40-nm-thick single crystal Cu/MgO layers is 0.8 to 1.2 nm, respectively, as determined by XRR measurements,[37] and is comparable to the roughness of the corresponding 20–40-nm-thick polycrystalline SG Cu layers. These roughness values cause a change in the net resistivity of 2–4% for the 40- to 20-nm-thick SC layers and ∼3.5% for the <40-nm-thick SG layers, based on Rossnagel and Kuan's formalism. These relatively small corrections (<4%) are within the experimental uncertainty data presented in Fig. 4 and are therefore not accounted for in the current analysis based on Eq. (3).

A corollary to Eq. (3) is that the contributions from electron scattering at surfaces and grain boundaries to the total resistivity cannot be separated from the effect of electron scattering by phonons (as well as crystalline point and line defects). However, the contribution from electron scattering at surfaces and grain boundaries can be quantified independently in Eq. (3)

TABLE I. Total resistivity ρ_f and relative contributions to the resistivity due to electron scattering by (i) phonons, (ii) phonons and surfaces, and (iii) phonons and grain boundaries of 20-, 30-, and 40-nm-thick single-crystal (SC), polycrystalline large-grain (LG) and small-grain (SG) Cu layers at 298 K. The table includes calculated values for samples with grain size D equal to the film thickness d ($D = d$). The last column illustrates the deviation of Eq. (3) from Matthiessen's rule.

				Electron scattering contribution			
		Grain size		(i) Phonons	(ii) Phonons and surfaces	(iii) Phonons and grain boundaries	
d_{Cu} (nm)	Sample	D (nm)	ρ_f ($\mu\Omega$-cm)	ρ_o/ρ_f	ρ_f^{sc}/ρ_f	ρ_g/ρ_f	$\frac{\rho_f^{sc}+\rho_g-\rho_o}{\rho_f}$
40	SC	∞	2.48	0.69	1.00		
	LG	200	2.67	0.64	0.92	0.70	0.98
	SG	110	2.85	0.60	0.87	0.70	0.97
	$D = d$	40	3.42	0.50	0.68	0.72	0.90
30	SC	∞	2.76	0.62	1.00		
	LG	176	3.00	0.57	0.91	0.63	0.97
	SG	97	3.23	0.53	0.86	0.64	0.97
	$D = d$	30	4.07	0.42	0.62	0.67	0.87
20	SC	∞	3.23	0.53	1.00		
	LG	147	3.60	0.47	0.90	0.53	0.96
	SG	81	3.90	0.44	0.83	0.54	0.93
	$D = d$	20	5.52	0.31	0.51	0.59	0.79

by studying the limiting cases of either completely specular scattering at interfaces ($p_1 = p_2 = 0$) or no reflection at grain boundaries ($R = 0$). Table I lists the relative contributions to the layer resistivity ρ_f solely due to electron scattering from (i) phonons (and bulk defects), (ii) phonons and surfaces, and (iii) phonons and grain boundaries in single-crystal and polycrystalline Cu layers for $d_{\text{Cu}} = 40$, 30, and 20 nm. The relative contributions are calculated using:

$$\text{Isotropic background: } \frac{\rho_o}{\rho_f} = \frac{\rho_f(R = 0, p_1 = p_2 = 1)}{\rho_f(R, p_1, p_2)}$$

$$\text{Background and surfaces: } \frac{\rho_f^{\text{sc}}}{\rho_f} = \frac{\rho_f(R = 0, p_1, p_2)}{\rho_f(R, p_1, p_2)} \quad (7)$$

Background and grain boundaries:

$$\frac{\rho_g}{\rho_f} = \frac{\rho_f(R, p_1 = p_2 = 1)}{\rho_f(R, p_1, p_2)}.$$

Here, ρ_o, ρ_f^{sc}, and ρ_g are the resistivities for bulk single-crystal Cu, a single-crystal Cu layer, and bulk polycrystalline Cu, respectively, and $\rho_f(R,\ p_1,\ p_2)$ is obtained from Eq. (3) using $R = 0.25$ for polycrystalline Cu layers and $p = 0$ for Cu-air, Cu-MgO, and Cu-Ta interfaces. We note that scattering at point defects and impurities is expected to contribute less than 1% to the resistivity of high-purity ($\geqslant$99.99%) Cu layers, according to Refs. 4 and 46, and is therefore neglected. Hence, $\rho_o = 1.71\ \mu\Omega$-cm used in calculations for Table I is entirely due to phonon scattering.[47] The data in Table I illustrates that the relative contribution due to phonon scattering decreases with both a decreasing layer thickness and a decreasing grain size. This is due to the increasing importance of surface and grain boundary scattering, respectively. A comparison of columns (ii) and (iii) for the SG and LG samples shows that the resistivity due to surface scattering is significantly greater than that due to grain boundary scattering. However, if the grain size is reduced by a factor of 3–5 so that it becomes equal to the layer thickness ($D = d$), as also shown in Table I from calculated values, electron scattering at grain boundaries dominates over surface scattering. This is in excellent agreement with experimental results by Sun *et al.*,[23,28] who also found grain boundary scattering to dominate for $D \sim d$. The last column in Table I illustrates the deviation of Eq. (3) from Matthiessen's rule. It corresponds to (ii) + (iii) − (i), which would yield a value of 1.0 if Matthiessen's rule would apply. All values for polycrystalline layers are <1.0, indicating that the effects of surface and grain boundary scattering are less than additive. This intuitively makes sense, since the effect of surface scattering decreases with a decreasing electron mean free path. That is, if additional grain boundaries decrease the electron mean free path due to both phonon and grain boundary scattering, the absolute contribution from electron surface scattering decreases, which in turn leads to $\rho_f^{\text{sc}} + \rho_g - \rho_o < \rho_f$. We note that the values in the last column for SG and LG are 0.96 ± 0.03; that is, the deviation from Matthiessen's rule is ~4%. This deviation is smaller than the experimental uncertainty, which is primarily due to uncertainties in the layer thickness. In addition, the correction associated with the layer roughness is, as discussed above, also of the order of ~4%. Thus, experimentally observing the deviation from Matthiessen's rule would require

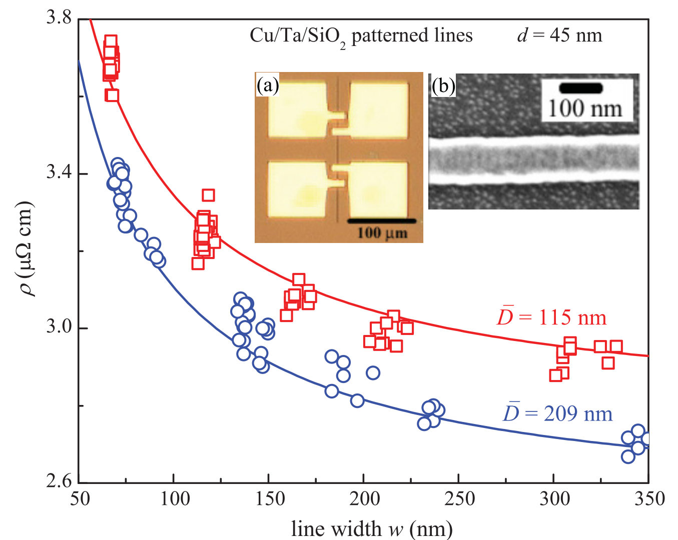

FIG. 5. (Color online) Resistivity ρ at 298 K vs line width w of 45-nm-thick SG and LG Cu wires with average grain size $\bar{D} = 115$ and 209 nm, respectively. Inset (a) is an optical micrograph of the 4-point probe contacts on a Cu wire with $w = 300$ nm, and inset (b) is a scanning electron micrograph of a Cu wire with $w = 117$ nm. The solid lines are obtained from simultaneous fitting using Eq. (6).

a considerably higher experimental accuracy and better control over surface roughness than what has been achieved in this paper.

D. Electron transport in Cu wires

Figure 5 is a plot of the resistivity ρ measured at 298 K vs the line width w of Cu wires obtained by patterning LG and SG 45-nm-thick Cu layers. The inset (a) is an optical microscope image of the 4-point probe pattern on a Cu wire. The wire is 300 nm wide and appears as a dark vertical line, while the four square-shaped e-beam patterned contact pads appear bright. The length between the two inner probes with which the voltage is measured is $l = 50\ \mu$m. A representative scanning electron micrograph of a Cu wire with $w = 117$ nm is shown in inset (b). The bright outline at the wire edges is due to charge buildup during imaging because of residual polymer resist. The plot shows that ρ of polycrystalline SG and LG wires increases with decreasing line width from 2.95 and 2.70 $\mu\Omega$-cm for $w =$ 340 nm to 3.62 and 3.38 $\mu\Omega$-cm for $w = 68$ nm, respectively. The lower ρ for LG-vs-SG wires is attributed to the larger average grain size for LG wires, as quantified by EBSD on Cu layers from which the nanowires were subtractively patterned, and hence less electron scattering at grain boundaries in LG than SG patterned Cu wires. The increase in ρ with decreasing w is primarily attributed to an increase in electron scattering at the Cu-air boundary at side walls and the dominance of highly resistive grain boundaries, as described by the additional semi-empirical boundary scattering term D/w in Eq. (6). The effect of impurities is expected to be negligible (<4%), based on previous work reported in Ref. 4. The solid lines in Fig. 5 are obtained by fitting the data with the expression in Eq. (6), using R as the only fitting parameter. For this purpose, the value for p is set to zero because the Cu-air and Cu-Ta interfaces

are known to cause completely diffuse electron scattering as described above,[10,12] and the average grain size $\bar{D}$ is fixed to 115 and 209 nm for the SG and LG wires, respectively, based on the grain size analysis for 45-nm-thick Cu layers described above. For the purpose of data analysis, we neglect roughness effects, which are expected to affect the resistivity of the $350 \times 45\text{-nm}^2$ SG wire by <4% and that of the corresponding LG wire by <9%, based on Rossnagel and Kuan's formalism and using the rms roughness values of 1.0 and 2.6 nm, respectively, from XRR measurements on the corresponding Cu layers. The fitting provides a value for R of 0.30 ± 0.05, which is in excellent agreement with the $R = 0.25 \pm 0.05$ for polycrystalline Cu films, indicating that Eq. (6) is appropriate to model the resistivity in metal nanowires. The best fit with the commonly used approximate FS + MS model for wires, that is, Eq. (6) without the semi-empirical term D/w, underestimates the resistivity with increasing error from 3% for $w = 350$ nm to 16% for $w = 50$ nm. The data in Fig. 5 also shows that the relative resistivity reduction from SG to LG wires, i.e. $(\rho_{SG} - \rho_{LG})/\rho_{SG}$, decreases from 9 to 7% as w decreases from 350 to 70 nm. This indicates that the relative conductivity gain associated with increasing the grain size becomes less important as the wire width decreases, which is attributed to a larger contribution of electron scattering at external surfaces for the narrower wires. We note, however, that this change is relatively small and could also be attributed to the increasing importance of the surface roughness, which is larger for the LG wires.

V. CONCLUSIONS

Combining electron transport data from polycrystalline and single-crystal Cu layers and nanowires with variable thickness, width, and grain size provides a systematic method to deconvolute the electron scattering contributions from grain boundaries and from top, bottom, and side surfaces. The experimental results demonstrate a 10–15% decrease in the resistivity of 30–50-nm-thick polycrystalline Cu layers when increasing the average grain size by a factor of 1.8. The corresponding decrease for 70–350-nm-wide and 45-nm-thick wires is by 7–9%. Additionally, the data also demonstrates, using single-crystal Cu layers, that the maximum resistivity decrease that can be achieved by increasing the grain size of polycrystalline 20–50-nm-thick SG Cu layers is 18–22%.

The commonly used approximate FS and MS expressions to describe surface and grain boundary scattering are accurate as long as the critical wire dimension is larger than the electron mean free path for phonon scattering. However, decreasing the wire cross section and layer thickness results in an increasing error that corresponds to the deviation from the commonly used resistivity expressions that are Eq. (6) without the semi-empirical term D/w for metal wires and Eq. (4) for metal thin films. The error for nanowires increases from 3% for $350 \times 45\ \text{nm}^2$ to 16% for $50 \times 45\ \text{nm}^2$, it increases for Cu layers from 6.5% for $d = 50$ nm to 17% for $d = 20$ nm. The exact Eq. (3) accurately describes the resistivity of polycrystalline Cu films and affirms the deviation from Matthiessen's rule, as quantified in Table I. The MS model is well suited to describe grain boundary scattering in wires where the wire width is larger than the average grain size. However, for narrow wires, an additional scattering term proportional to D/w is required, in order to account for the large variation in the specific resistivity of different grain boundaries.

ACKNOWLEDGMENTS

The authors acknowledge Marko Radosavljevic and Benjamin Chu-Kung, Intel Corporation, for help with e-beam lithography. The authors also acknowledge Scott Baumann, Materials Characterization Services (Austin, Texas) for EBSD measurements. The portion of research carried out at Rensselaer Polytechnic Institute has been supported by the National Science Foundation, under Grant No. 0645312.

*galld@rpi.edu

[1] A. C. Longden, Phys. Rev. (Ser. 1) **11**, 40 (1900).
[2] *ITRS 2010 Update* (International Technology Roadmap for Semiconductors, 2010), http://www.itrs.net/Links/2010ITRS/Home2010.htm.
[3] W. Steinhogl, G. Schindler, G. Steinlesberger, and M. Engelhardt, Phys. Rev. B **66**, 075414 (2002).
[4] J. J. Plombon, E. Andideh, V. M. Dubin, and J. Maiz, Appl. Phys. Lett. **89**, 113124 (2006).
[5] D. Josell, S. H. Brongersma, and Z. Tokei, Annu. Rev. Mater. Res. **39**, 231 (2009).
[6] K. Fuchs, Proc. Cambridge Philos. Soc. **34**, 100 (1938).
[7] E. H. Sondheimer, Adv. Phys. **1**, 1 (1952).
[8] S. M. Rossnagel and T. S. Kuan, J. Vac. Sci. Technol. B **22**, 240 (2004).
[9] J. M. Purswani and D. Gall, Thin Solid Films **516**, 465 (2007).
[10] J. S. Chawla and D. Gall, Appl. Phys. Lett. **94**, 252101 (2009).
[11] V. Timoshevskii, Y. Ke, H. Guo, and D. Gall, J. Appl. Phys. **103**, 113705 (2008).
[12] J. S. Chawla, F. Zahid, H. Guo, and D. Gall, Appl. Phys. Lett. **97**, 132106 (2010).
[13] M. Hein and D. Schumacher, J. Phys. D **28**, 1937 (1995).
[14] E. F. McCullen, C. L. Hsu, and R. G. Tobin, Surf. Sci. **481**, 198 (2001).
[15] E. T. Krastev, D. E. Kuhl, and R. G. Tobin, Surf. Sci. **387**, L1051 (1997).
[16] F. Zahid, Y. Q. Ke, D. Gall, and H. Guo, Phys. Rev. B **81**, 045406 (2010).
[17] A. F. Mayadas, M. Shatzkes, and J. F. Janak, Appl. Phys. Lett. **14**, 345 (1969).
[18] S. B. Soffer, J. Appl. Phys. **38**, 1710 (1967).
[19] R. B. Dingle, Proc. R. Soc. London Ser. A **201**, 545 (1950).
[20] T. H. Kim, X. G. Zhang, D. M. Nicholson, B. M. Evans, N. S. Kulkarni, B. Radhakrishnan, E. A. Kenik, and A. P. Li, Nano Lett. **10**, 3096 (2010).

[21]E. T. Krastev, L. D. Voice, and R. G. Tobin, J. Appl. Phys. **79**, 6865 (1996).
[22]A. F. Mayadas and M. Shatzkes, Phys. Rev. B **1**, 1382 (1970).
[23]T. Sun, B. Yao, A. P. Warren, K. Barmak, M. F. Toney, R. E. Peale, and K. R. Coffey, Phys. Rev. B **79**, 041402 (2009).
[24]J. M. E. Harper, C. Cabral, P. C. Andricacos, L. Gignac, I. C. Noyan, K. P. Rodbell, and C. K. Hu, J. Appl. Phys. **86**, 2516 (1999).
[25]R. L. Graham, G. B. Alers, T. Mountsier, N. Shamma, S. Dhuey, S. Cabrini, R. H. Geiss, D. T. Read, and S. Peddeti, Appl. Phys. Lett. **96**, 042116 (2010).
[26]H. Marom, J. Mullin, and M. Eizenberg, Phys. Rev. B **74**, 045411 (2006).
[27]W. Wu, S. H. Brongersma, M. Van Hove, and K. Maex, Appl. Phys. Lett. **84**, 2838 (2004).
[28]T. Sun, B. Yao, A. P. Warren, K. Barmak, M. F. Toney, R. E. Peale, and K. R. Coffey, Phys. Rev. B **81**, 155454 (2010).
[29]R. C. Munoz, J. P. Garcia, R. Henriquez, A. M. Moncada, A. Espinosa, M. Robles, G. Kremer, L. Moraga, S. Cancino, J. R. Morales, A. Ramirez, S. Oyarzun, M. A. Suarez, D. Chen, E. Zumelzu, and C. Lizama, Phys. Rev. Lett. **96**, 206803 (2006).
[30]R. Henriquez, S. Cancino, A. Espinosa, M. Flores, T. Hoffmann, G. Kremer, J. G. Lisoni, L. Moraga, R. Morales, S. Oyarzun, M. A. Suarez, A. Zuniga, and R. C. Munoz, Phys. Rev. B **82**, 113409 (2010).
[31]R. C. Munoz, M. A. Suarez, S. Oyarzun, R. Henriquez, A. Espinosa, G. Kremer, L. Moraga, S. Cancino, and R. Morales, Phys. Rev. B **81**, 165408 (2010).
[32]B. Feldman, S. Park, M. Haverty, S. Shankar, and S. T. Dunham, Phys. Status Solidi B **247**, 1791 (2010).
[33]J. M. Purswani, T. Spila, and D. Gall, Thin Solid Films **515**, 1166 (2006).
[34]G. R. Jones, M. Jackson, and K. O'Grady, J. Magn. Magn. Mater. **193**, 75 (1999).
[35]F. J. Humphreys, J. Mater. Sci. **36**, 3833 (2001).
[36]S. H. Brongersma, E. Richard, I. Vervoort, H. Bender, W. Vandervorst, S. Lagrange, G. Beyer, and K. Maex, J. Appl. Phys. **86**, 3642 (1999).
[37]J. S. Chawla, X. Y. Zhang, and D. Gall, J. Appl. Phys. **110**, 043714 (2011).
[38]A. F. Mayadas, R. Feder, and R. Rosenberg, J. Vac. Sci. Technol. **6**, 690 (1969).
[39]J. W. Lim, K. Mimura, and M. Isshiki, Appl. Surf. Sci. **217**, 95 (2003).
[40]J. M. Thijssen, H. J. F. Knops, and A. J. Dammers, Phys. Rev. B **45**, 8650 (1992).
[41]J. M. Thijssen, Phys. Rev. B **51**, 1985 (1995).
[42]M. E. Straumanis and L. S. Yu, Acta Crystallogr. Sec. A **A25**, 676 (1969).
[43]R. Lacombe, *Adhesion Measurement Methods: Theory and Practice* (CRC Press, Boca Raton, Florida, 2006), p. 378.
[44]B. Feldman and S. T. Dunham, Appl. Phys. Lett. **95**, 222101 (2009).
[45]T. S. Kuan, C. K. Kinoki, G. S. Oerlein, K. Rose, Y. P. Zhao, G. C. Wang, S. M. Rossnagel, and C. Cabral, Mater. Res. Soc. Online Proc. Library **No. 612**, D7.1.1. (2000).
[46]J. W. Lim and M. Isshiki, J. Appl. Phys. **99**, 094909 (2006).
[47]D. R. Lide, *CRC Handbook of Chemistry and Physics*, 84th ed. (CRC Press, Boca Raton, Florida, 2003), Sec. 12, p. 41.